


## Article

# Hydrogeochemical Characteristics and Evolution Processes of Karst Groundwater Affected by Multiple Influencing Factors in a Karst Spring Basin, Eastern China

Shuai Gao<sup>1,2,3,\*</sup> , Changsuo Li<sup>1,2,3,\*</sup>, Yuanyuan Liu<sup>4</sup>, Bin Sun<sup>1,2,3</sup>, Zhiqiang Zhao<sup>1,2,3</sup>, Minghui Lv<sup>1,2,3</sup> and Shiting Gang<sup>1,2,3</sup>

- <sup>1</sup> 801 Institute of Hydrogeology and Engineering Geology, Shandong Provincial Bureau of Geology & Mineral Resources, Jinan 250014, China; spinh1r@163.com (B.S.); zzq0912@163.com (Z.Z.); lmhyoxiang@163.com (M.L.); gangshenting@163.com (S.G.)
- <sup>2</sup> Shandong Engineering Research Center for Environmental Protection and Remediation on Groundwater, Jinan 250014, China
- <sup>3</sup> Key Laboratory of Groundwater Resources and Environment, Shandong Provincial Bureau of Geology & Mineral Resources, Jinan 250014, China
- <sup>4</sup> Administrative Office, Shandong Polytechnic College, Jining 272067, China; belinda9999@126.com
- \* Correspondence: shuaigao90@126.com (S.G.); lics120@163.com (C.L.)

**Abstract:** Karst groundwater is an important water supply, especially in northern China. With the rapid development of China's economy, anthropogenic activities have had a significant impact on karst groundwater formation, circulation and other processes. In this paper, the Baotu spring basin, which is closely related to anthropogenic activities, was selected as the research object to carry out a study of water chemical characteristics and evolutionary processes. And, mathematical statistics, Piper trilinear diagram, Gibbs diagram, and ion ratio methods were used to analyze the characteristics and evolution processes of groundwater. The results of this study show that the hydrogeochemical components of karst groundwater are mainly controlled by the weathering of rocks, mainly by the dissolution of carbonate rocks and silicates with the dominant cation of  $\text{Ca}^{2+}$  and the dominant anion of  $\text{HCO}_3^-$ . Considering the role of anthropogenic activities, including agricultural and industrial activities, the evolution process of karst groundwater is mainly controlled by hydrogeochemical effects such as mineral dissolution and filtration, the mixing of multiple water bodies, anthropogenic activities (domestic sewage, industrial and agricultural wastes), oxidation–reduction and cation alternating adsorption. Moreover, the influence of anthropogenic activities on the formation and evolution of karst groundwater gradually increases, leading to the rise in nitrate content in karst groundwater and accelerating carbonate rock dissolution. The research results of this paper can provide a favorable reference for environmental protection and research on karst groundwater in areas of intensive anthropogenic activity.



**Citation:** Gao, S.; Li, C.; Liu, Y.; Sun, B.; Zhao, Z.; Lv, M.; Gang, S. Hydrogeochemical Characteristics and Evolution Processes of Karst Groundwater Affected by Multiple Influencing Factors in a Karst Spring Basin, Eastern China. *Water* **2023**, *15*, 3899. <https://doi.org/10.3390/w15223899>

Academic Editor: Elias Dimitriou

Received: 14 September 2023

Revised: 1 November 2023

Accepted: 4 November 2023

Published: 8 November 2023

**Keywords:** karst groundwater; hydrogeochemical characteristics; evolution processes; anthropogenic activities; eastern China



**Copyright:** © 2023 by the authors. Licensee MDPI, Basel, Switzerland. This article is an open access article distributed under the terms and conditions of the Creative Commons Attribution (CC BY) license (<https://creativecommons.org/licenses/by/4.0/>).

## 1. Introduction

Water resources are essential basic resources for human economic and social development, among which karst groundwater resources provide living and production water resources for nearly 1/4 of the global population [1]. Thus, the quantity and quality of karst groundwater are very sensitive issues worldwide, affected by meteorological factors and geological factors. However, anthropogenic activity, such as excessive groundwater exploitation, water conservation structure, and alterations in land use/landcover patterns, have significantly altered the hydrogeochemical processes of karst groundwater with the increase in population, the expansion of cities and the development of industry and agriculture [2–4]. In China, karst aquifers are widely distributed in the north and south of

China, providing abundant good-quality groundwater for living, agricultural irrigation, and ecology [5,6]. Especially in the north, karst groundwater resources provide sufficient water for living, industry and agriculture in large and middle cities. In recent decades, the hydrodynamic and hydrogeochemical processes of karst groundwater have undergone great changes with the increasing anthropogenic activity in the north of China, which affects the utilization of karst groundwater by causing declines in its quantity and quality [7]. In this case, it is necessary to re-examine the hydrogeological process of karst groundwater in order to better protect and utilize karst groundwater in northern China.

Groundwater's hydrogeochemical evolution in the karst area has the characteristics of complexity, fuzziness, and uncertainty due to the heterogeneity and anisotropy of carbonate strata, which largely depend on natural processes, such as hydrogeological conditions, lithology, the mineral composition of the aquifer and water–rock interactions when anthropogenic activity is less intrusive [4,8–11]. However, at present, anthropogenic activity and climate change have obviously affected the hydrogeochemical evolution of groundwater around the world [2,3,12,13]. There are numerous techniques for evaluating the evolution processes of groundwater with the development of the hydrogeochemical research field. The analysis of hydrogeochemical components, such as via the Piper three-line diagram, the Gibbs model, ion correlation, end-member diagrams and geochemical modeling, is a crucial method to master the characteristics of groundwater based on hydrogeochemical principles [14–16]. For example,  $\text{Ca}^{2+}$ ,  $\text{Mg}^{2+}$  and  $\text{HCO}_3^-$  generally come from the dissolution of carbonate rocks; of course, some  $\text{Ca}^{2+}$  may also come from the dissolution of gypsum.  $\text{Na}^+$  and  $\text{Cl}^-$  are mainly derived from atmospheric sedimentation and halite dissolution in natural conditions. Nevertheless, anthropogenic inputs are a significant factor affecting the concentration of these ions, as well as that of  $\text{NO}_3^-$  [17,18]. In addition to mineral dissolution, mixing, cation alternating adsorption and REDOX are also important factors affecting the hydrogeochemical process of karst groundwater. At the present stage, the analysis of hydrogeochemical components has become an indispensable tool to research the hydrogeochemical processes of karst water.

The Baotu Spring basin (BTSB) is an important karst water system in northern China, deriving its value from resources, tourism, humans and ecology. In recent decades, urban expansion and population growth led to increased groundwater extraction and changes in the recharge conditions. The water level of karst groundwater decreased to the lowest level in the 1980s and karst springs stopped outflowing. After the 2000s, this situation was improved through the implementation of a series of artificial control measures [19–22]. However, the hydrogeochemical process of karst groundwater has changed a great deal in BTSB compared to before. Thus, the research purpose of this paper is to analyze the characteristics and relationships of karst water, fissure water, pore water and surface water, explain the influencing factors for characteristics of these water bodies and reidentify the hydrogeochemical evolution processes of the typical karst groundwater system. This can improve the knowledge of the regional water cycle, providing important evidence for the utilization of karst groundwater and ecological protection for karst springs.

## 2. Materials and Methods

### 2.1. Description of the Study Area

BTSB is located in the middle of Jinan City, Shandong Province, which belongs to the warm temperate continental monsoon climate zone. The annual average temperature is about 14.2 °C, and the annual average precipitation is about 646.55 mm according to data (1959–2019) from the China Meteorological Data Service Centre. The annual precipitation distribution shows obvious seasonality, with more precipitation from June to September and less precipitation from December to May of the next year. The terrain is high in the southeast and low in the northwest. The south is a middle and low elevation mountainous area, and the north is a sloping plain in the piedmont. The absolute elevation is reduced from 500 m~600 m to 25 m~50 m from south to north [23]. The main rivers in the area include the Yellow River, Yufu River, and Beidasha River; the main lakes are the Wohushan

Reservoir, Jinxiuchuan reservoir, and Gushan reservoir. Yufu River and Beidasha River form the Yellow River tributaries from southeast to northwest into the Yellow River [24,25].

BTSB is a monoclinical structure that is high in the south and low in the north, located at the junction of the northern margin of Mountain Tai and the piedmont inclined plain. The eastern and western parts of BTSB are bounded by the Dongwu fault and Mashan fault, which are water-blocking faults [26]. The southern boundary is the surface–underground watershed of Mountain Tai, and the northern boundary is the 400 m buried line of Ordovician limestone roof [27]. As shown in Figure 1, the Cambrian and Ordovician carbonate strata of Paleozoic cover the metamorphic rock series of Neoproterozoic Taishan Group and are buried under the Quaternary system of Cenozoic, the Carboniferous system and the Permian system of the Late Paleozoic. The dip direction of strata is basically consistent with the topographic aspect that tends toward the northwest direction. The intrusive rock of Yanshanian period is distributed over a large area in the northern urban area, providing the geological basis for the formation of Jinan springs groups. The study area is divided into a direct recharge area, indirect recharge area and discharge area from south to north, and each functional area plays an important role in karst groundwater formation and circulation. Gneiss and carbonate strata are directly exposed on the surface in the direct recharge area and indirectly on the recharge area, with lots of vertical cracks, which lead to atmospheric precipitation directly recharging groundwater. Yufu River and Beidasha River are also closely connected with groundwater, meaning that leakages can reach 7.96 m<sup>3</sup>/s and 1.23 m<sup>3</sup>/s, respectively, from river water to groundwater in the wet season. Thus, these rivers are important recharge sources for karst groundwater. Cambrian and Ordovician carbonate strata are primary aquifers of karst groundwater, which develop complex fissure networks consisting of karst caves, fissures and pores. The Cambrian carbonate aquifer and Ordovician carbonate aquifer form an aquifer because they have uniform groundwater levels connected through permeable faults and vertical fissures. The hydrogeological information of the main aquifer was obtained via pumping tests and geological drillings. The hydraulic conductivity of the Cambrian carbonate aquifer and Ordovician carbonate aquifer showed strong spatial anisotropy, with a maximum hydraulic conductivity of 570 m/d; a hydraulic conductivity of 0 m/d~10 m/d accounts for 63%, a conductivity of 10 m/d~20 m/d accounts for 8%, and a conductivity greater than 20 m/d accounts for 29%. The Quaternary sand aquifer is mainly distributed in the western and northern areas, with a maximum hydraulic conductivity of 130 m/d, where the hydraulic conductivity of 0 m/d~10 m/d accounts for 47%, a conductivity of 10 m/d~20 m/d accounts for 19%, and a conductivity greater than 20 m/d accounts for 34%.

Generally, groundwater moves from south to north along the slope direction of the terrain and the dip direction of strata, and is blocked by the intrusive rock masses in the urban area. Part of the groundwater flows out to the ground in the form of springs along the vertical karst channels and fissures of the strata. The other part forms a deep circulation, moving down the strata to the north of the Yellow River to form geothermal water [28,29].

According to the characteristics of groundwater storage space, groundwater in BTSB can be divided into karst water, fissure water and pore water (Figure 1). Karst water is mainly distributed in the middle and northern part of the study area and karst aquifer consists of Cambrian and Ordovician strata, whose lithology is mainly limestone and dolomite. Karst water has characteristics of a fast flow and high update rate because of its karst channels and fissure network. Pore water is mainly distributed in the piedmont inclined plain, slightly inclined low plain and intermountain plain in the northern part of BTSB (Figure 1). Porous aquifer mainly consists of Quaternary strata whose lithology is mainly clay and silty clay. Pore water has the characteristics of slow flow and a low update rate that is limited by its storage and transport pores. Fissure water is mainly distributed in the middle and low mountains in the southern area, whose fissure aquifer consists of Archaean intrusive rocks and metamorphic rocks mainly composed of gneiss and granite. Fissure water has the characteristics of a medium flow and update rate in which its storage and transport space (fissure network) is primarily distributed in weathered

crust [19,27,30,31]. In addition, there is a close hydraulic connection between surface water and groundwater in the area, and karst water is easily polluted by the infiltration of surface water. Thus, surface water is also an important part of karst groundwater's evolution processes [21,32].

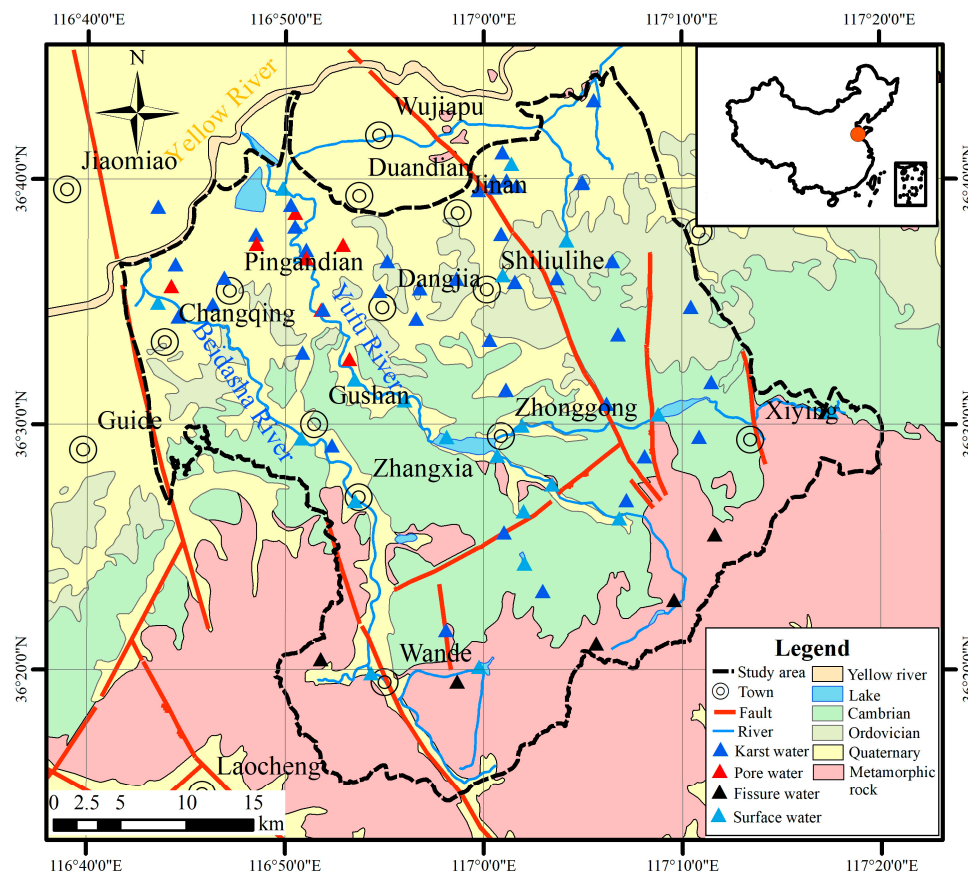


**Figure 1.** Geological map of study area including sampling sites.

## 2.2. Sample Collection and Measurements

In order to master the hydrogeochemical process of karst groundwater, 55 groundwater samples (include 7 pore water samples, 6 fissure water samples, 42 karst water samples) and 20 surface water samples were sampled in the study area (Figure 1) in September 2021. Groundwater samples are mainly collected from groundwater environment monitoring wells and groundwater supply wells. The groundwater was pumped out at about triple the wellbore volume, aiming to purge stagnant water and acquire fresh groundwater that flows into the wellbore. Polyethylene bottles of 2.5 L were cleaned with fresh groundwater three times before formal sampling to avoid contaminating the samples with impurities in the bottle. Sampling bottles were filled without air bubbles and sealed with a parafilm membrane to reduce the effects of evaporation and external pollution. All samples were immediately stored in coolers at 4 °C and delivered to the lab within 12 h. Surface water samples were collected using a peristaltic pump. The inlet of the peristaltic pump was placed 0.5 m below the water surface in the middle of a lake and a river. The peristaltic pump pumped lake or river water for 5 min, avoiding contamination caused by remnant water in the pipeline. Similarly, the 2.5 L polyethylene bottles were cleaned with fresh groundwater three times before formal sampling to avoid contaminating the samples with impurities in the bottle. The requirements of sample protection and transportation were the same as those for groundwater.

The main ions were measured in the hydrochemistry laboratory of Shandong Provincial Geo-mineral Engineering Exploration Institute. The main anions ( $\text{Cl}^-$ ,  $\text{SO}_4^{2-}$ ,  $\text{NO}_3^-$ )

were measured using ion chromatography (ICS-600 ion chromatography, Thermo Fisher, Waltham, MA, USA) with an analytical precision 0.007 mg/L, 0.046 mg/L, 0.016 mg/L, respectively. The main cations ( $K^+$ ,  $Na^+$ ,  $Ca^{2+}$ ,  $Mg^{2+}$ ) were measured using inductively coupled plasma emission spectrometer (Optima 7000 DV, PerkinElmer, Glen Waverley VIC, Australia) with an analytical precision of 0.05 mg/L, 0.12 mg/L, 0.02 mg/L, and 0.02 mg/L, respectively.  $HCO_3^-$  was analyzed via hydrochloric acid titration. pH was measured using Benchtop pH meter (Orion Star™ A211, Thermo Fisher, Waltham, MA, USA) with an analytical precision of 0.01. TDS (Total Dissolved Solids) is calculated using anion and cation data. All measurements were checked using the ion balance test for accuracy, which was estimated using Equation (1); the measured results were reliable with a relative error (E) within  $\pm 5\%$ :

$$E(\%) = \frac{\sum N_c - \sum N_a}{\sum N_c + \sum N_a} \times 100 \quad (1)$$

where E is relative error, no unit; and  $N_c$ ,  $N_a$  are the milligram equivalent concentration of anion and cation, respectively, meq/L.

After calculation, the relative error (E) of measurements was within 5%, indicating that the measurements are reliable.

### 3. Results and Discussion

#### 3.1. Characteristics of Major Chemical Components

In order to understand the hydrogeochemical characteristics of groundwater and surface water, the concentrations of major chemical components were counted, including minimum (Min), maximum (Max), Mean, standard deviation (SD) and coefficient of variation (CV). Descriptive statistical results are shown in Table 1.

**Table 1.** Descriptive statistics of hydrogeochemical components.

Water Type	Parameters	pH	TDS mg/L	$K^+$ mg/L	$Na^+$ mg/L	$Ca^{2+}$ mg/L	$Mg^{2+}$ mg/L	$Cl^-$ mg/L	$SO_4^{2-}$ mg/L	$HCO_3^-$ mg/L	$NO_3^-$ mg/L
Surface water	Min	7.60	209.04	1.36	6.74	38.00	8.46	12.70	49.50	95.03	0.77
	Max	8.20	609.59	4.07	41.20	143.00	24.40	70.90	153.00	275.91	92.70
	Mean	7.97	364.62	2.44	16.31	80.08	15.14	26.23	84.47	204.94	23.83
	SD	0.18	92.80	0.81	8.98	23.55	4.25	15.00	25.99	53.32	18.33
	CV	0.02	0.25	0.33	0.55	0.29	0.28	0.57	0.31	0.26	0.77
Pore water	Min	7.40	499.10	0.34	12.30	52.59	15.30	35.70	32.70	236.05	14.00
	Max	7.80	1533.47	2.36	95.90	76.55	48.10	269.00	235.00	665.24	192
	Mean	7.59	724.00	1.21	43.27	67.02	25.24	102.97	110.16	363.42	78.50
	SD	0.13	364.10	0.81	30.65	8.51	11.12	80.32	79.95	160.26	65.52
	CV	0.02	0.50	0.66	0.71	0.13	0.44	0.78	0.73	0.44	0.83
Fissure water	Min	6.90	248.48	0.89	10.20	52.20	7.53	14.50	30.50	107.30	0.66
	Max	7.60	497.72	3.55	24.70	109.00	28.60	50.70	83.80	335.73	75.40
	Mean	7.27	345.08	1.96	17.00	71.25	14.76	23.12	57.20	198.64	34.69
	SD	0.28	91.69	1.01	5.55	26.36	7.85	14.22	20.68	98.96	26.19
	CV	0.04	0.27	0.52	0.33	0.37	0.53	0.62	0.36	0.50	0.76
Karst water	Min	7.20	203.09	0.21	2.29	13.30	6.28	11.40	20.40	92.73	0.51
	Max	8.80	899.84	13.40	59.10	209.00	29.50	106.00	239.00	486.01	199
	Mean	7.60	490.42	1.54	21.70	94.80	18.77	43.91	90.90	279.31	42.37
	SD	0.30	163.68	2.37	14.06	43.35	5.43	24.72	45.89	70.14	37.43
	CV	0.04	0.33	1.54	0.65	0.46	0.29	0.56	0.50	0.25	0.88

TDS and pH are two important parameters reflecting the quality of groundwater. The pH values of surface water ranged from a minimum of 7.60 to a maximum of 8.20, with an average of 7.97, which had the characteristics of low alkalinity. The concentration of TDS ranged from 209.04 mg/L to 609.59 mg/L, with an average of 364.62 mg/L (Table 1). The dominant cation of surface water was  $Ca^{2+}$ , whose concentration varied from 38.00 mg/L

to 143.00 mg/L, with an average of 80.08 mg/L (Figure 2d). The concentration order of the remaining cations was  $\text{Na}^+ > \text{Mg}^{2+} > \text{K}^+$ , which implied that surface water may be under the influence of urban and rural sewage in karst areas. The dominant anion was  $\text{HCO}_3^-$ , whose concentration varied between 95.03 mg/L and 275.91 mg/L, with an average of 204.94 mg/L. The concentration order of the other anions was  $\text{SO}_4^{2-} > \text{Cl}^- > \text{NO}_3^-$ , whose concentration of  $\text{SO}_4^{2-}$  may be related to the sulfate fertilizer. Moreover, the coefficient of variation of  $\text{Na}^+$  and  $\text{Cl}^-$  was larger than that of other ions, implying the local pollution of surface water caused by anthropogenic activities.

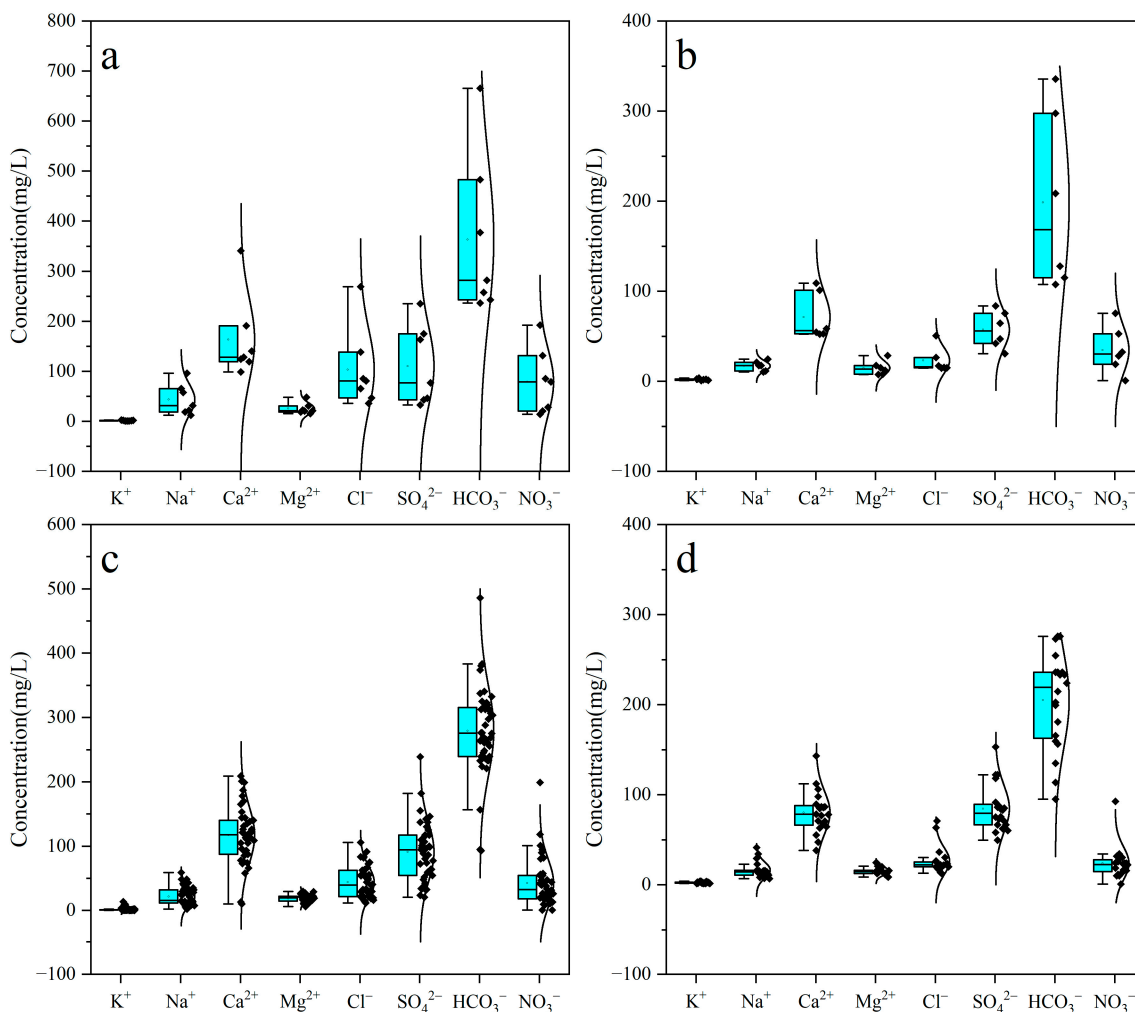


**Figure 2.** Box diagram concentrations of major element of pore water (a), fissure water (b), karst water (c), and surface water (d).

The pH values of pore water had a range of 7.40~7.80, with an average of 7.59, reflecting the characteristic of low alkalinity. The concentration of TDS ranged from a minimum of 499.10 mg/L to a maximum of 1533.47 mg/L, with an average of 724.00 mg/L, characteristic of a large distribution range and high concentration (Table 1). The dominant cation of pore water was also  $\text{Ca}^{2+}$ , whose concentration varied from 52.59 mg/L to 76.55 mg/L, with an average of 67.02 mg/L (Figure 2a). The concentration order of the remaining cations is  $\text{Na}^+ > \text{Mg}^{2+} > \text{K}^+$ , with atmospheric precipitation leaching pollutants from anthropogenic activities into pore water aquifers, resulting in a high  $\text{Na}^+$  concentration. The dominant anion was  $\text{HCO}_3^-$ , whose concentration ranged from a minimum of 236.05 mg/L to a maximum of 665.24 mg/L, with an average of 363.42 mg/L. The concentrations of  $\text{Cl}^-$  and  $\text{SO}_4^{2-}$  were almost identical and the  $\text{NO}_3^-$  values were relatively low, with a large coefficient of variation. The coefficient of variation of each ion concentration in pore water was

relatively large, especially in  $\text{Na}^+$ ,  $\text{K}^+$ ,  $\text{Cl}^-$ ,  $\text{NO}_3^-$  and  $\text{SO}_4^{2-}$ . In summary, pore water was mainly controlled by mineral dissolution, but anthropogenic activities seriously affected the hydrogeochemical composition of pore water.

Fissure water aquifers are distributed in a relatively independent area in the southern part of the study area, with less urban distribution. The pH values of fissure water ranged from a minimum of 6.90 to a maximum of 7.60, with an average of 7.27, which had the characteristic of low alkalinity. The concentration of TDS varied between 248.48 mg/L and 497.72 mg/L, with an average of 345.08 mg/L (Table 1). The dominant cation of fissure water was  $\text{Ca}^{2+}$ , which ranged from 52.20 mg/L to 109.00 mg/L, with an average of 71.25 mg/L (Figure 2b). The concentrations of other cations were relatively low, with a concentration order of  $\text{Na}^+ > \text{Mg}^{2+} > \text{K}^+$ , which may be related to albite dissolution. The dominant anion was  $\text{HCO}_3^-$ , whose concentration ranged from a minimum of 107.30 mg/L to a maximum of 335.73 mg/L, with an average of 198.64 mg/L. Overall, the ion concentrations of fissure water had a lower value and smaller coefficient of variation than other water bodies, and were mainly controlled by natural hydrogeochemical processes.

Karst water aquifers are the main aquifer in the study area and the research emphasis of this paper. The pH values of karst water ranged from a minimum of 7.20 to a maximum of 8.80, with an average of 7.60, with the characteristic of low alkalinity. The concentration of TDS varied between 203.09 mg/L and 899.84 mg/L, with an average of 490.42 mg/L (Table 1). The dominant cation was  $\text{Ca}^{2+}$ , whose concentration ranged from 13.30 mg/L to 209.00 mg/L, with an average of 94.80 mg/L (Figure 2c). The concentrations of other cations were relatively low, with a concentration order of  $\text{Na}^+ > \text{Mg}^{2+} > \text{K}^+$ .  $\text{HCO}_3^-$  was the dominant anion of karst water, whose concentration ranged from 92.73 mg/L to 486.01 mg/L, with an average of 279.31 mg/L. The concentrations of other anions were relatively high, with the order of  $\text{SO}_4^{2-} > \text{Cl}^- > \text{NO}_3^-$ , and had a relatively large coefficient of variation.

### 3.2. Hydrogeochemical Type

The Piper trilinear diagram is an effective tool to classify water types and analyze the evolution of water [33–35]. A comprehensive Piper plot was drawn according to the hydrogeochemical component concentrations of pore water, fissure water, karst water and surface water. Zones I, II, III, IV in the upper rhombus represent alkaline earth exceeding alkalis and weak acid exceeding strong acid ( $\text{HCO}_3\text{-Ca}\cdot\text{Mg}$  type), alkaline earth exceeding alkalis and strong acid exceeding weak acid ( $\text{SO}_4\text{-Cl}\text{-Ca}\cdot\text{Mg}$  type), alkalis exceeding alkaline earth and strong acid exceeding weak acid ( $\text{SO}_4\text{-Cl}\text{-Na}$  type), and alkalis exceeding alkaline earth and weak acid exceeding strong acid ( $\text{HCO}_3\text{-Na}$  type), respectively. Zones A, B, C, D, E, F, G in the following two triangles represent calcium type, no dominant type, magnesium type, sodium and potassium type, bicarbonate type, sulphate type, and chloride type, respectively.

As shown in Figure 3, pore water samples were mainly distributed in zones I and II in the Piper trilinear diagram, representing  $\text{HCO}_3\text{-Ca}\cdot\text{Mg}$  type (four samples) and  $\text{SO}_4\text{-Cl}\text{-Ca}\cdot\text{Mg}$  type (three samples). Anthropogenic activities may influence the characteristics of pore water because the pore water aquifer is the uppermost strata. Fissure water samples were also mainly distributed in zones I and II, representing the  $\text{HCO}_3\text{-Ca}\cdot\text{Mg}$  type (five samples) and the  $\text{SO}_4\text{-Cl}\text{-Ca}\cdot\text{Mg}$  type (one samples). The dissolution of mineral may be mainly controlled by the process of the fissure water's hydrogeochemical component. Karst water samples had a dispersed distribution in zones I, II, and III, where the hydrogeochemical types of karst water are relatively complex. A total of 34 karst water samples were of the  $\text{HCO}_3\text{-Ca}\cdot\text{Mg}$  type, accounting for 81% of the total. Seven karst water samples were of the  $\text{SO}_4\text{-Cl}\text{-Ca}\cdot\text{Mg}$  type. Only one sample was of the  $\text{SO}_4\text{-Cl}\text{-Na}$  type. This indicates that karst water experienced a complex evolutionary process, controlled by hydrogeochemical processes and anthropogenic activities [36]. Surface water samples (Figure 2) were mainly distributed in zones I and II, representing  $\text{HCO}_3\text{-Ca}\cdot\text{Mg}$  type (19 samples)

and  $\text{SO}_4\text{-Cl-Ca-Mg}$  type (1 sample), showing that the water–rock interaction is a main influencing factor.

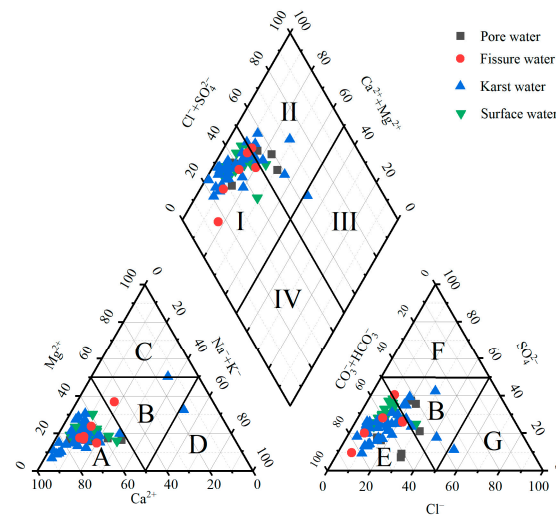


**Figure 3.** Piper trilinear diagram for groundwater and surface water.

### 3.3. Water–Rock Interaction

The Gibbs model diagram (Figure 4a,b) is widely used to analyze the natural processes driving hydrochemistry in water, although it cannot reflect the influences of anthropogenic activities [37]. The Gibbs diagram shows the relationship of  $\text{Na}^+ / (\text{Na}^+ + \text{Ca}^{2+})$  and  $\text{Cl}^- / (\text{Cl}^- + \text{HCO}_3^-)$  to TDS, reflecting the hydrogeochemical components of samples controlled by evaporation, rock weathering or atmospheric precipitation. All groundwater samples and surface water samples distributed in the rock weathering zone, and surface water samples showed an evolutionary trend toward the evaporation zone, which suggests that the hydrogeochemical components of groundwater and surface water were primarily controlled by rock weathering and surface water was affected by evaporation and concentration (Figure 4a,b). A scatter plot of  $\text{Ca}^{2+} / \text{Na}^+$  vs.  $\text{Mg}^{2+} / \text{Na}^+$  and  $\text{Ca}^{2+} / \text{Na}^+$  vs.  $\text{HCO}_3^- / \text{Na}^+$  can explain why hydrogeochemical components are controlled by the dissolution of carbonate, silicates or evaporation [38]. Pore water, fissure water and surface samples were distributed between silicates and carbonates but closer to silicates, reflecting that they are more controlled by the dissolution of silicates than carbonates [39]. Karst water samples distributed more widely between silicates and carbonates, indicating that multi-source mixing resulted in karst water samples moving closer to silicates (Figure 4c,d). Therefore, the dissolution of carbonates and silicates is the main controlling factor for groundwater and surface water in the study area.

In order to further analyze the control effect of the dissolution of carbonates and silicates on hydrogeochemical components, it is essential to analyze stratigraphic lithology and potential hydrogeochemical processes. This study area is located in the stratigraphic division of western Shandong Province, which is mainly composed of metamorphic rocks of the Taishan Group and Cambrian–Ordovician carbonate rocks. The Taishan Group is mainly composed of gneiss, hornblende and granite, and its main mineral components include biotite, potassium feldspar, plagioclase, quartz, and hornblende. The Cambrian–Ordovician system is mainly dolomite and limestone, whose main mineral components are calcite, dolomite, containing a small amount of gypsum, quartz, and clay minerals according to a regional hydrogeological survey report. The hydrogeochemical composition of groundwater and surface water is mainly controlled by the dissolution reactions of the above minerals [40].



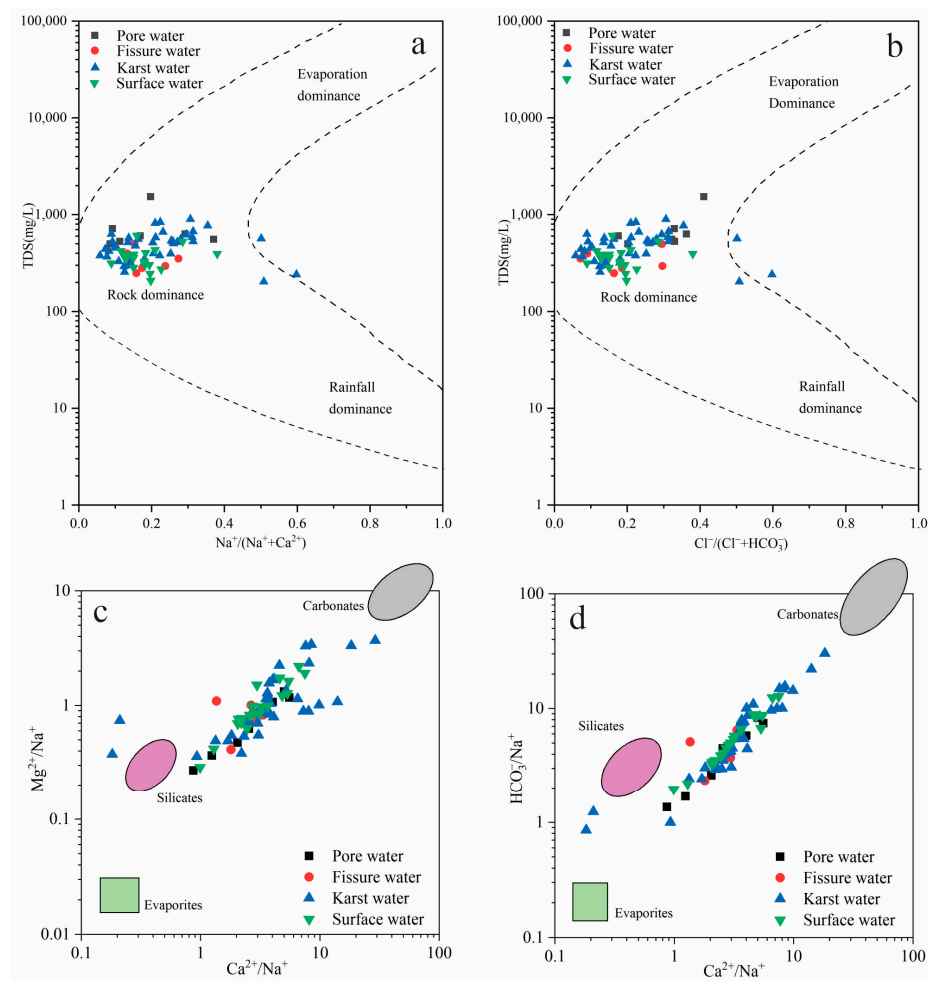
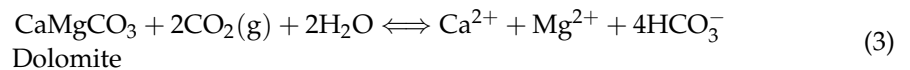
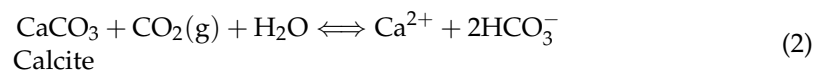
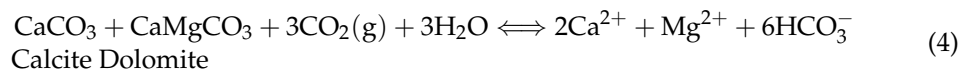


**Figure 4.** Gibbs diagram and three-member diagram of water samples. (a)  $\text{Na}^+ / (\text{Na}^+ + \text{Ca}^{2+})$  vs. TDS; (b)  $\text{Cl}^- / (\text{Cl}^- + \text{HCO}_3^-)$  vs. TDS; (c)  $\text{Ca}^{2+} / \text{Na}^+$  vs.  $\text{Mg}^{2+} / \text{Na}^+$ ; (d)  $\text{Ca}^{2+} / \text{Na}^+$  vs.  $\text{HCO}_3^- / \text{Na}^+$ .

In the presence of  $\text{CO}_2$ , the dissolution equation of calcite and dolomite is as follows:



If both calcite and dolomite participate in the dissolution process, the dissolution reaction is as follows:



According to the dissolution equations of calcite and dolomite, the ratio of  $(\text{Ca}^{2+} + \text{Mg}^{2+}) / \text{HCO}_3^-$  should be 1:1 when  $\text{Ca}^{2+}$ ,  $\text{Mg}^{2+}$  and  $\text{HCO}_3^-$  are entirely derived from calcite and dolomite. In this study, all samples were distributed at the lower right of the 1:1 line in the scatter plot of  $(\text{Ca}^{2+} + \text{Mg}^{2+}) / \text{HCO}_3^-$  and had a positive correlation (Figure 5a). This indicates that groundwater and surface water may be affected by minerals

containing  $\text{Ca}^{2+}$  and  $\text{Mg}^{2+}$ , such as gypsum, except calcite and dolomite. The dissolution equation of gypsum is as follows:

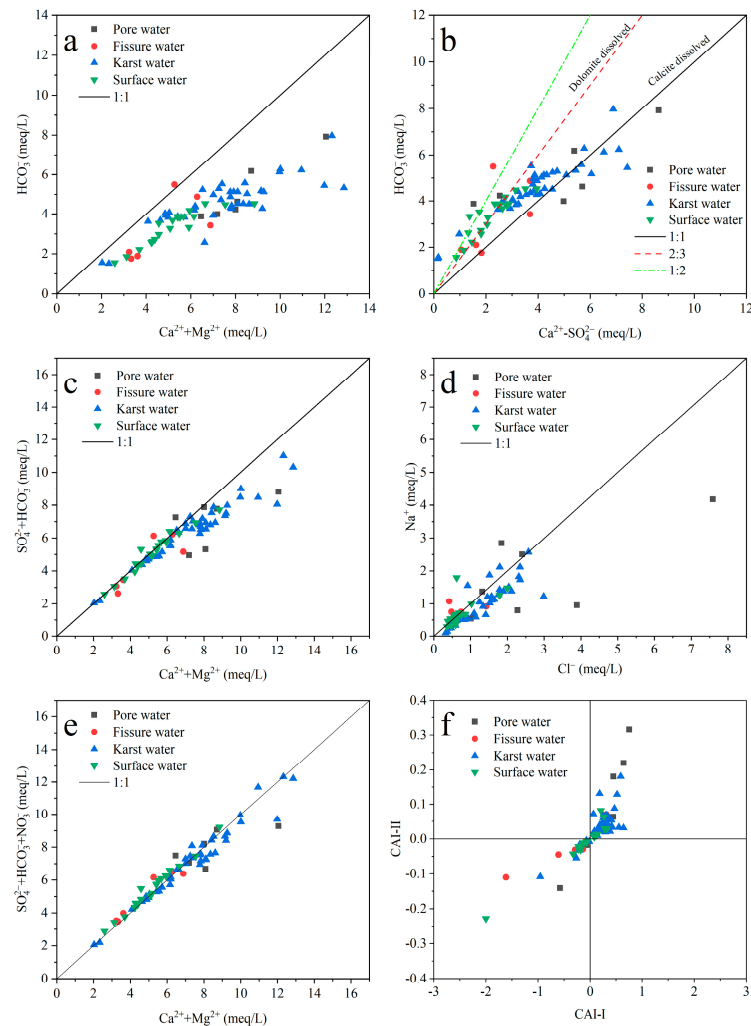
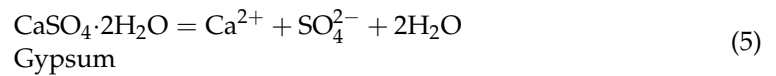


**Figure 5.** Analysis of the ion ratio in water samples. (a) Scatter plot of  $\text{Ca}^{2+} + \text{Mg}^{2+}$  vs.  $\text{HCO}_3^-$ ; (b)  $\text{Ca}^{2+} + \text{Mg}^{2+}$  vs.  $\text{SO}_4^{2-} + \text{HCO}_3^-$ ; (c)  $\text{Ca}^{2+} - \text{SO}_4^{2-}$  vs.  $\text{HCO}_3^-$ ; (d)  $\text{Cl}^-$  vs.  $\text{Na}^+$ ; (e)  $\text{Ca}^{2+} + \text{Mg}^{2+}$  vs.  $\text{SO}_4^{2-} + \text{HCO}_3^- + \text{NO}_3^-$ ; (f) chlor-alkali index CAI-I vs. CAI-II.

Thus, it is necessary to determine whether the dissolution of gypsum affects the hydro-geochemical composition of groundwater and surface water. The ratio of  $(\text{Ca}^{2+} + \text{Mg}^{2+}) / (\text{SO}_4^{2-} + \text{HCO}_3^-)$  is used to determine whether gypsum is involved in dissolution, together with calcite and dolomite. Scatters of groundwater and surface samples approached the 1:1 line, showing that the dissolution of gypsum does exist (Figure 5c). Otherwise, with the increase in  $\text{Ca}^{2+} + \text{Mg}^{2+}$ , the karst water gradually deviated from the 1:1 line downward, which may be caused by the increase in the dissolution of gypsum, cation exchange, or other hydrogeochemical process along the runoff path. The dispersion of pore water and fissure water was larger than that of karst water and surface water, indicating that a complex geological composition may be an important factor affecting the concentration of these ions in pore water and fissure water.

According to the dissolution equations of calcite and dolomite, the ratio of  $\text{Ca}^{2+} / \text{HCO}_3^-$  can be used to identify the dissolution degree of calcite and dolomite. However, in reality,

the dissolution of gypsum and silicate in the stratum and cation exchange in the aquifer can also affect the  $\text{Ca}^{2+}$  concentration in groundwater and surface water. Therefore, it is assumed that the effect of gypsum dissolution on  $\text{Ca}^{2+}$  concentration is much greater than that of cation exchange in this study. Thus, the ratios of  $(\text{Ca}^{2+} - \text{SO}_4^{2-})/\text{HCO}_3^-$  can explain why the dissolution of calcite is dominant or the dissolution of dolomite is dominant. When the ratio of  $(\text{Ca}^{2+} - \text{SO}_4^{2-})/\text{HCO}_3^-$  is close to 1:1, only calcite is dissolved, excluding the effect of gypsum dissolution. When the ratio of  $(\text{Ca}^{2+} - \text{SO}_4^{2-})/\text{HCO}_3^-$  is close to 1:2, only dolomite is dissolved. When calcite and dolomite dissolve at the same time, there are two conditions: the dissolution of calcite is preponderant, so that the ratio ranges between 1:1 and 2:3; the dissolution of dolomite is preponderant, so that the ratio ranges between 2:3 and 1:2. Karst water, pore water, and surface water were mainly controlled by dolomite dissolution when the ion content was low, but shifted to being mainly controlled by calcite dissolution as the ion concentration increased. This may be due to differences in the composition of major minerals in the strata during the runoff process. On the other hand, this phenomenon also suggested that karst water, pore water, and surface water may have a certain hydraulic connection. Additionally, the complexity of the mineral composition of the formation in the fissure water region, and the large difference in the proportion of  $\text{Ca}^{2+}$  and  $\text{HCO}_3^-$  produced by the dissolution reaction, led to the discrete distribution of fissure water samples.

Scatter plots of  $(\text{Ca}^{2+} + \text{Mg}^{2+})/\text{HCO}_3^-$  show that  $\text{Ca}^{2+} + \text{Mg}^{2+}$  and  $\text{HCO}_3^-$  have a positive correlation trend and most water samples are plotted under the 1:1 line, which indicates that the dissolution of carbonate rocks plays an important role and  $\text{Ca}^{2+}$  and  $\text{Mg}^{2+}$  have other sources (Figure 5a). The mineral source of  $\text{Ca}^{2+}$  may originate from evaporites like gypsum and anhydrite, except for carbonate rocks. Scatter plots of  $(\text{Ca}^{2+} + \text{Mg}^{2+})/(\text{SO}_4^{2-} + \text{HCO}_3^-)$  can account for the dissolution of dolomite, calcite and gypsum or anhydrite. Most scatters of the  $(\text{Ca}^{2+} + \text{Mg}^{2+})/(\text{SO}_4^{2-} + \text{HCO}_3^-)$  plot become closer to the 1:1 line, indicating that gypsum or anhydrite do participate in dissolution (Figure 5c). However, karst water and surface water scatters still deviate from the line when the concentration of  $\text{Ca}^{2+} + \text{Mg}^{2+}$  exceeds 8.0 meq/L, at which point the dissolution of gypsum may increase or the dissolution of carbonate may increase under the action of other strong acids. Figure 5b shows that surface water and karst sample evolve from a predominantly dolomite dissolution to a predominantly calcite dissolution with the increase in  $\text{Ca}^{2+} - \text{SO}_4^{2-}$ . Some samples are beyond the range of the ion proportion dissolved by dolomite and calcite, which indicates that there are other complicated hydrogeochemical processes, in addition to carbonate and gypsum dissolution.

The  $\text{Na}^+$  and  $\text{Cl}^-$  in water may originate from the dissolution of halite and silicate or the cation exchange adsorption. If only halite is dissolved in water, the milligram equivalent ratio of  $\text{Na}^+$  and  $\text{Cl}^-$  should be equal to 1 [41]. Most of the  $\text{Na}^+$  and  $\text{Cl}^-$  ions in pore water deviated from the 1:1 line, indicating that the source of  $\text{Na}^+$  and  $\text{Cl}^-$  ions in pore water was complicated, which may be influenced by the dissolution of halite, silicate and anthropogenic activities. Karst water samples were mainly distributed below the 1:1 line and parallel to the 1:1 line.  $\text{Cl}^-$  is a stable element in nature, which is neither adsorbed by minerals nor absorbed by vegetation. However, the concentration of  $\text{Na}^+$  decreased overall in karst water due to other factors (cation exchange adsorption, clay mineral adsorption of cation, etc.), which explained the distribution trend of karst water samples in Figure 5d. Surface water samples basically fell on the 1:1 line, indicating that  $\text{Na}^+$  and  $\text{Cl}^-$  in surface water mainly came from the dissolution of halite. Moreover, the distribution of fissure water samples was relatively discrete, indicating that  $\text{Na}^+$  and  $\text{Cl}^-$  in fissure water mainly originate from albite and halite [39].

### 3.4. REDOX Action

In the process of groundwater circulation, as there is sufficient dissolved oxygen in atmospheric precipitation and surface water in the recharge area, the water body is in a strong oxidation state.  $\text{NH}_4^+$  in the water body that is leached from agricultural land or

urban wastewater will be oxidized into  $\text{NO}_3^-$ , and the  $\text{NO}_3^-$  formed in this process will also increase the dissolution of carbonate rocks [31]. With the groundwater runoff, the dissolved oxygen in groundwater is constantly consumed and its content continuously decreases. When the free oxygen is exhausted,  $\text{NO}_3^-$  will become the first electron acceptor to be utilized, and the microorganisms with facultative characteristics will continuously transform  $\text{NO}_3^-$  into  $\text{NO}_2^-$ , and eventually into  $\text{N}_2$ , which is the process of denitrification. This process will cause a reduction in the  $\text{NO}_3^-$  content in water. Therefore, the analysis of nitrate changes with groundwater runoff and its dissolution with carbonate rocks can qualitatively recognize the REDOX action in the water body in the study area.

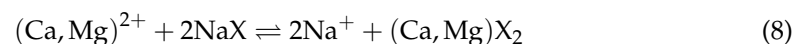
$\text{NH}_4^+$  in the water body will be oxidized to  $\text{NO}_3^-$ , and the  $\text{NO}_3^-$  formed in this process will also increase the dissolution of carbonates. Therefore, the comparison between  $\text{Ca}^{2+} + \text{Mg}^{2+}$  vs.  $\text{SO}_4^{2-} + \text{HCO}_3^- + \text{NO}_3^-$  and  $\text{Ca}^{2+} + \text{Mg}^{2+}$  vs.  $\text{SO}_4^{2-} + \text{HCO}_3^-$  can reflect the sample points or regions where  $\text{NO}_3^-$  participates in the dissolution of carbonates. The explanation of this problem needs to meet the following conditions: First, there is domestic sewage, animal feces and other pollution. Second, groundwater contains dissolved oxygen. Third, the dissolved mineral around the water body is carbonate. By comparing Figures 5c and 5e, karst water and pore water samples were shown to deviate from the line to the lower right when the concentration of  $\text{Ca}^{2+} + \text{Mg}^{2+}$  exceeded 8.0 meq/L in Figure 5c, and all deviated sample points were close to the 1:1 line in Figure 5e, indicating that the nitric acid content of karst water and pore water was increased due to the REDOX action. Thus, dissolved minerals, especially carbonate, increase dissolution, causing an increase in the concentration of  $\text{Ca}^{2+} + \text{Mg}^{2+}$ . Surface water had the same trend, but this was not obvious when the concentration of  $\text{Ca}^{2+} + \text{Mg}^{2+}$  exceeded 8.0 meq/L. The REDOX effect is not obvious in fissure water, maybe because fissure water is less affected by anthropogenic activities.

### 3.5. Cation Exchange

Cationic exchange is the process of cation exchange between groundwater and the surrounding aquifer medium, which is subject to ionic charge, hydration radius and other conditions [36,42]. The chlor-alkali index is usually used to analyze whether there is cation exchange and adsorption in groundwater [43], and this parameter is calculated by using the milligram equivalent concentration of each ion (Formulas (6) and (7)). If  $\text{Ca}^{2+}$  and  $\text{Mg}^{2+}$  in groundwater exchange with  $\text{Na}^+$  ions in aquifer minerals, Equation (8) goes to the right and both chlor-alkali coefficients are negative. If the opposite ion exchange process occurs, Equation (8) goes to the left and both chlor-alkali coefficients are positive.

$$\text{CAI - I} = \frac{\text{Cl}^- - (\text{Na}^+ + \text{K}^-)}{\text{Cl}^-} \quad (6)$$

$$\text{CAI - II} = \frac{\text{Cl}^- - (\text{Na}^+ + \text{K}^-)}{\text{SO}_4^{2-} + \text{HCO}_3^- + \text{CO}_3^{2-} + \text{NO}_3^-} \quad (7)$$



The reverse cation exchange occurred in most of the karst water and pore water samples, resulting in a relative decrease in  $\text{Na}^+$  ion content in the samples, and a relative increase in  $\text{Ca}^{2+}$  and  $\text{Mg}^{2+}$  (Figure 5f). Only a few samples underwent a positive cation exchange in karst water and pore water. Surface water samples were relatively complex; about half of each sample had a positive and negative cation exchange, but the ion exchange capacity was generally small. Figure 5f shows that the fissure water was mainly dominated by positive cation exchange, which was an influencing factor when the concentration of  $\text{Na}^+$  in fissure water samples was more than that of  $\text{Ca}^{2+}$ . Certainly, the dissolution of albite in fissure water was the main influencing factor for this phenomenon.

### 3.6. Anthropogenic Activity

The hydrogeochemical components of groundwater and surface water, especially  $\text{SO}_4^{2-}$ ,  $\text{Cl}^-$  and  $\text{NO}_3^-$ , are not only controlled by natural factors, but are also strongly influenced by anthropogenic activities [36,44]. At present, the main anthropogenic activities affecting the hydrogeochemical components of groundwater and surface water in the study area are the discharge of agricultural fertilizer, industrial wastewater and domestic sewage. Generally speaking, the concentration of nitrate groundwater or surface water is very low if nitrate originates from atmospheric sedimentation. However, some anthropogenic activities can significantly increase its concentration, such as factory wastewater, animal feces, and agricultural fertilizers [45]. The  $\text{Cl}^-/\text{Na}^+$  and  $\text{NO}_3^-/\text{Na}^+$  ratios in a water body controlled by the dissolution of carbonates and silicates are both naturally very low, while the high  $\text{Cl}^-/\text{Na}^+$  and  $\text{NO}_3^-/\text{Na}^+$  ratios are usually related to agricultural fertilizers. The  $\text{Cl}^-/\text{Na}^+$  ratio will be close to 0.7 and the  $\text{NO}_3^-/\text{Na}^+$  ratio close to 0 if the water body is significantly affected by urban sewage. Additionally, the  $\text{Cl}^-/\text{Na}^+$  ratio will be close to 1, indicating that evaporation is a major influencing factor for nitrates and chlorides in the water body [46–48]. Moreover, the plot of  $\text{SO}_4^{2-}/\text{Ca}^{2+}$  and  $\text{NO}_3^-/\text{Na}^+$  can be used to confirm that nitrate and sulfate originate from agricultural activity, industrial activity, or domestic sewage [48].

In this study area, pore water, fissure water, karst water, and surface water were all close to the end element of agricultural pollution, which shows that the nitrate in most surface water and groundwater samples originated from agricultural activities (Figure 6a). One fissure water sample, one surface water sample, and two karst water samples were close to the end element of urban sewage, which may be partially affected by urban sewage. In addition, all samples have the characteristics of low  $\text{SO}_4^{2-}/\text{Ca}^{2+}$  and a wide range of  $\text{NO}_3^-/\text{Na}^+$ , which reconfirm that the nitrate in most surface water and groundwater samples originated from agricultural activities (Figure 6b).

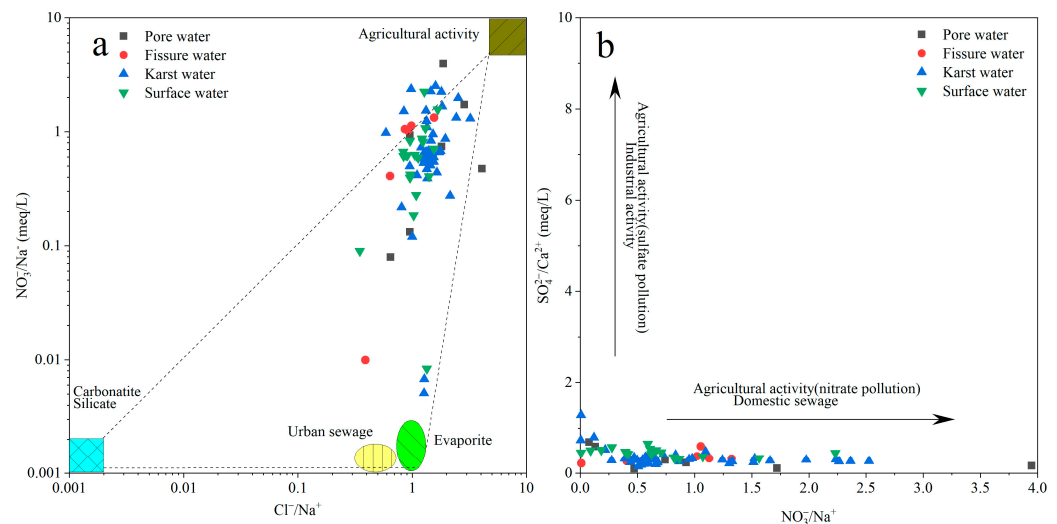


**Figure 6.** Analysis of anthropogenic activities. (a)  $\text{Cl}^-/\text{Na}^+$  vs.  $\text{NO}_3^-/\text{Na}^+$ ; (b)  $\text{NO}_3^-/\text{Na}^+$  vs.  $\text{SO}_4^{2-}/\text{Ca}^{2+}$ .

However, from the perspective of local economic development, the fissure water is distributed in fruit plantations and cultivated land distribution areas, such as walnut, kiwi, and wheat, and the agricultural activities are relatively active. Pore water is distributed in the western part of the study area, where cultivated land is almost entirely distributed. Therefore, it is more obviously polluted by agricultural fertilizers (Figure 6a). Karst water is distributed in the northern and central parts of the study area, which are the most densely populated areas. Additionally, the evaporite mineral content in strata is very small according to the hydrogeological conditions. Thus, according to Figure 6a,b, agricultural activities are the most important factors influencing the increase in nitrate

content in karst water, which is related to the inorganic or organic fertilizers used in agricultural activities such as urea ( $(\text{NH}_2)_2\text{CO}$ ), ammonium sulfate ( $(\text{NH}_4)_2\text{SO}_4$ ), ammonium nitrate ( $\text{NH}_4\text{NO}_3$ ), monoammonium phosphate ( $\text{NH}_4\text{H}_2\text{PO}_4$ ), and diammonium phosphate ( $(\text{NH}_4)_2\text{HPO}_4$ ) [36].

#### 4. Conclusions

The main purpose of this study is to reveal the hydrogeochemical characteristics and main influencing factors of karst groundwater in the Baotu spring basin, a karst spring basin in Eastern China. In addition, the hydrogeochemical characteristics and main influencing factors of surface water, pore water, and fissure water were analyzed in order to better analyze the characteristics of karst groundwater. This paper can draw the following conclusions through comprehensive analysis.

The hydrogeochemical components of various water bodies are mainly controlled by water–rock interactions, where the geological components of the aquifer are the dominant control factors. REDOX action, cation exchange and anthropogenic activity are secondary factors that lead to increases in the complexity of the hydrogeochemical components of various water bodies. The concentration of hydrogeochemical components in fissure water is the lowest, while that of pore water is the highest, and karst water is in the middle. Moreover, the variation coefficient of various ion contents in pore water is larger than in other water types, indicating that shallow groundwater is more susceptible to multiple factors. Additionally, anthropogenic activities seriously affect the hydrogeochemical composition of pore water and added vales, which confirms this statement.

The formation of karst water is mainly controlled by the dissolution of carbonate rocks and silicates. Considering the role of anthropogenic activities, the evolution process of karst groundwater is mainly controlled by hydrogeochemical effects such as mineral dissolution and filtration, the mixing of multiple water bodies, anthropogenic activities (domestic sewage, industrial and agricultural wastes), oxidation reduction, and cation exchange. It is worth noting that the influence of anthropogenic activities on the formation and evolution of karst groundwater gradually increased, especially agricultural activities, which caused the quality of karst groundwater to deteriorate, such as by increasing the concentration of nitrate and sulfate. Furthermore, nitrate from anthropogenic activities is involved in the dissolution process of carbonate in the study area when the concentration of  $\text{Ca}^{2+} + \text{Mg}^{2+}$  exceeds 8.0 meq/L, which indicates that anthropogenic activities seriously affect the composition of karst groundwater. Therefore, the research on aquifer protection and efficient agricultural management should be strengthened in future water resource management in this study area.

**Author Contributions:** Conceptualization, S.G. (Shuai Gao) and C.L.; methodology, S.G. (Shuai Gao); software, Y.L.; validation, Y.L. and B.S.; formal analysis, Z.Z.; investigation, S.G. (Shiting Gang); resources, C.L.; data curation, S.G. (Shiting Gang) and M.L.; writing—original draft preparation, S.G. (Shiting Gang); writing—review and editing, S.G. (Shuai Gao) and C.L.; visualization, S.G. (Shiting Gang); supervision, Z.Z.; project administration, S.G. (Shuai Gao); funding acquisition, S.G. (Shuai Gao). All authors have read and agreed to the published version of the manuscript.

**Funding:** This research was supported by the National Natural Science Foundation of China (42202294), Shandong Provincial Natural Science Foundation (ZR2021QD084), Geological exploration and Science and Technology Project of Shandong Provincial Bureau of Geology & Mineral Resources (KY202217).

**Data Availability Statement:** Not applicable.

**Acknowledgments:** We thank the reviewers and editors for their pertinent comments.

**Conflicts of Interest:** The authors declare no conflict of interest.

## References

1. Ford, D.; Williams, P. *Karst Hydrogeology and Geomorphology*; John Wiley & Sons: Chichester, UK, 2007.
2. Laveti, N.V.S.; Banerjee, A.; Kartha, S.A.; Dutta, S. Anthropogenic influence on monthly groundwater utilization in an irrigation dominated Ganga river Sub-Basin. *J. Hydrol.* **2021**, *593*, 125800. [[CrossRef](#)]
3. Wang, S.; Lee, C.; Yeh, C.; Choo, Y.F.; Tseng, H. Evaluation of Climate Change Impact on Groundwater Recharge in Groundwater Regions in Taiwan. *Water* **2021**, *13*, 1153. [[CrossRef](#)]
4. Liu, Z.; Feng, S.; Zhang, D.; Han, Y.; Cao, R. Effects of precipitation, irrigation, and exploitation on groundwater geochemical evolution in the people's victory canal irrigation area, China. *Appl. Water Sci.* **2023**, *13*, 1. [[CrossRef](#)]
5. He, K.; Jia, Y.; Wang, F.; Lu, Y. Overview of karst geo-environments and karst water resources in north and south China. *Environ. Earth Sci.* **2011**, *64*, 1865–1873. [[CrossRef](#)]
6. Liang, Y.; Gao, X.; Zhao, C.; Tang, C.; Shen, H.; Wang, Z.; Wang, Y. Review: Characterization, evolution, and environmental issues of karst water systems in Northern China. *Hydrogeol. J.* **2018**, *26*, 1371–1385. [[CrossRef](#)]
7. Shen, H.; Xu, Y.; Liang, Y.; Zhao, C.; Wang, Z.; Zhang, Z.; Qi, J. Review: Groundwater recharge estimation in northern China karst regions. *Carbonates Evaporites* **2023**, *38*, 16. [[CrossRef](#)]
8. Moore, P.J.; Martin, J.B.; Screaton, E.J. Geochemical and statistical evidence of recharge, mixing, and controls on spring discharge in an eogenetic karst aquifer. *J. Hydrol.* **2009**, *376*, 443–455. [[CrossRef](#)]
9. Newman, C.P.; Paschke, S.S.; Keith, G. Natural and Anthropogenic Geochemical Tracers to Investigate Residence Times and Groundwater–Surface-Water Interactions in an Urban Alluvial Aquifer. *Water* **2021**, *13*, 871. [[CrossRef](#)]
10. Gibbs, R.J. Mechanisms controlling world water chemistry. *Science* **1970**, *170*, 1088–1090. [[CrossRef](#)]
11. Apollaro, C.; Marini, L.; De Rosa, R.; Settembrino, P.; Scarciglia, F.; Vecchio, G. Geochemical features of rocks, stream sediments, and soils of the Fiume Grande Valley (Calabria, Italy). *Environ. Geol.* **2007**, *52*, 719–729. [[CrossRef](#)]
12. Wang, W.; Chena, Y.; Chena, Y.; Wang, W.; Zhang, T.; Qin, J. Groundwater dynamic influenced by intense anthropogenic activities in a dried-up river oasis of Central Asia. *Hydrol. Res.* **2022**, *53*, 532. [[CrossRef](#)]
13. Stigter, T.Y.; Miller, J.; Chen, J.; Re, V. Groundwater and climate change: Threats and opportunities. *Hydrogeol. J.* **2023**, *31*, 7–10. [[CrossRef](#)]
14. Owor, M.; Muwanga, A.; Tindimugaya, C.; Taylor, R.G. Hydrogeochemical processes in groundwater in Uganda: A national-scale analysis. *J. Afr. Earth Sci.* **2021**, *175*, 104113. [[CrossRef](#)]
15. Yuan, H.; Yang, S.; Wang, B. Hydrochemistry characteristics of groundwater with the influence of spatial variability and water flow in Hetao Irrigation District, China. *Environ. Sci. Pollut. Res.* **2022**, *29*, 71150–71164. [[CrossRef](#)] [[PubMed](#)]
16. Apollaro, C.; Fuoco, I.; Gennaro, E.; Giuliani, L.; Iezzi, G.; Marini, L.; Radica, F.; Di Luccio, F.; Ventura, G.; Vespasiano, G. Advanced argillic alteration at Cave di Caolino, Lipari, Aeolian Islands (Italy): Implications for the mitigation of volcanic risks and the exploitation of geothermal resources. *Sci. Total Environ.* **2023**, *889*, 164333. [[CrossRef](#)] [[PubMed](#)]
17. Walraevens, K.; Bakundukize, C.; Mtoni, Y.E.; Van Camp, M. Understanding the hydrogeochemical evolution of groundwater in Precambrian basement aquifers: A case study of Bugesera region in Burundi. *J. Geochem. Explor.* **2018**, *188*, 24–42. [[CrossRef](#)]
18. Liu, J.; Wang, H.; Jin, D.; Xu, F.; Zhao, C. Hydrochemical characteristics and evolution processes of karst groundwater in Carboniferous Taiyuan formation in the Pingdingshan coalfield. *Environ. Earth Sci.* **2020**, *79*, 151. [[CrossRef](#)]
19. Zhang, Z.; Wang, W.; Qu, S.; Huang, Q.; Liu, S.; Xu, X.; Ni, L. A New Perspective to Explore the Hydraulic Connectivity of Karst Aquifer System in Jinan Spring Catchment, China. *Water* **2018**, *10*, 1368. [[CrossRef](#)]
20. Liu, W.; Zhang, L.; Liu, P.; Qin, X.; Shan, X.; Yao, X. FDOM Conversion in Karst Watersheds Expressed by Three-Dimensional Fluorescence Spectroscopy. *Water* **2018**, *10*, 1427. [[CrossRef](#)]
21. Luo, Q.; Yang, Y.; Qian, J.; Wang, X.; Chang, X.; Ma, L.; Li, F.; Wu, J. Spring protection and sustainable management of groundwater resources in a spring field. *J. Hydrol.* **2020**, *582*, 124498. [[CrossRef](#)]
22. Jiang, A.; Liu, Y.; Yi, S.; Guo, Z.; Cui, Y.; Huang, Q.; Li, J.; Liu, K.; Qiu, M.; Jin, X. Impact of artificial recharge on groundwater and springs: Jinan, China, case study. *Arab. J. Geosci.* **2021**, *14*, 111. [[CrossRef](#)]
23. Sun, K.; Hu, L.; Liu, X. The influences of sponge city construction on spring discharge in Jinan city of China. *Hydrol. Res.* **2020**, *51*, 959–975. [[CrossRef](#)]
24. Deng, X.; Xing, L.; Zhang, F.; Xing, X.; Zhang, Y.; Yu, M.; Liu, S.; Pan, W. Mapping regional and nested flow systems in the karst aquifers of Jinan spring using hydrochemical and isotope data. *Water Supply* **2023**, *23*, 3323. [[CrossRef](#)]
25. Kang, F.; Jin, M.; Qin, P. Sustainable yield of a karst aquifer system: A case study of Jinan springs in northern China. *Hydrogeol. J.* **2011**, *19*, 851–863. [[CrossRef](#)]
26. Xi, D.; Sun, B.; Qin, P. *Research on Jinan Spring*; Jinan Press: Jinan, China, 2017.
27. Guo, Y.; Qin, D.; Sun, J.; Li, L.; Huang, J. Recharge of River Water to Karst Aquifer Determined by Hydrogeochemistry and Stable Isotopes. *Water* **2019**, *11*, 479. [[CrossRef](#)]
28. Wang, J.; Jin, M.; Jia, B.; Kang, F. Hydrochemical characteristics and geothermometry applications of thermal groundwater in northern Jinan, Shandong, China. *Geothermics* **2015**, *57*, 185–195. [[CrossRef](#)]
29. Guo, F.; Guo, J.; Wang, C.; Fan, W.; Li, C.; Zhao, L.; Li, H.; Li, J. Formation of mafic magmas through lower crustal AFC processes—An example from the Jinan gabbroic intrusion in the North China Block. *Lithos* **2013**, *179*, 157–174. [[CrossRef](#)]
30. Meng, Q.; Xing, L.; Liu, L.; Xing, X.; Zhao, Z.; Zhang, F.; Li, C. Time-lag characteristics of the response of karst springs to precipitation in the northern China. *Environ. Earth Sci.* **2021**, *80*, 348. [[CrossRef](#)]

31. Wang, J.; Jin, M.; Lu, G.; Zhang, D.; Kang, F.; Jia, B. Investigation of discharge-area groundwaters for recharge source characterization on different scales: The case of Jinan in northern China. *Hydrogeol. J.* **2016**, *24*, 1723–1737. [[CrossRef](#)]
32. Zhang, Z.; Wang, W. Managing aquifer recharge with multi-source water to realize sustainable management of groundwater resources in Jinan, China. *Environ. Sci. Pollut. Res.* **2021**, *28*, 10872–10888. [[CrossRef](#)]
33. Piper, A.M. A graphic procedure in the geochemical interpretation of water-analyses. *Eos Trans. Am. Geophys. Union* **1944**, *25*, 914–928. [[CrossRef](#)]
34. Wang, M.; Zhang, W.; Yang, P.; Feng, J.; Zhang, R.; Gao, Z.; Jin, H.; Song, X.; Gao, X. Hydrogeochemical Characteristics, Water Quality, and Human Health Risks of Groundwater in Wulian, North China. *Water* **2023**, *13*, 359. [[CrossRef](#)]
35. Qu, S.; Liao, F.; Wang, G.; Wang, X.; Shi, Z.; Liang, X.; Duan, L.; Liu, T. Hydrochemical evolution of groundwater in overburdened aquifers under the influence of mining activity: Combining hydrochemistry and groundwater dynamics analysis. *Environ. Earth Sci.* **2023**, *85*, 135. [[CrossRef](#)]
36. Yang, Y.; Mei, A.; Gao, S.; Zhao, D. Both natural and anthropogenic factors control surface water and groundwater chemistry and quality in the Ningxia coalfield of Ordos Basin, Northwestern China. *Environ. Sci. Pollut. Res.* **2023**, *30*, 67227–67249. [[CrossRef](#)] [[PubMed](#)]
37. Yang, F.; Liu, S.; Jia, C.; Gao, M.; Chang, W.; Wang, Y. Hydrochemical characteristics and functions of groundwater in southern Laizhou Bay based on the multivariate statistical analysis approach. *Estuar. Coast. Shelf Sci.* **2021**, *250*, 107153. [[CrossRef](#)]
38. Zhang, X.; Zhao, R.; Wu, X.; Mu, W. Hydrogeochemistry, identification of hydrogeochemical evolution mechanisms, and assessment of groundwater quality in the southwestern Ordos Basin, China. *Environ. Sci. Pollut. Res.* **2022**, *29*, 901–921. [[CrossRef](#)] [[PubMed](#)]
39. Gaillardet, J.; Dupré, B.; Louvat, P.; Allegre, C.J. Global silicate weathering and CO<sub>2</sub> consumption rates deduced from the chemistry of large rivers. *Chem. Geol.* **1999**, *159*, 3–30. [[CrossRef](#)]
40. Zhang, H.; Yang, Y.; Qi, H.; Lu, Y.; Yu, T. Hydrochemical evolution of rare cold mineral waters in the Wudalianchi UNESCO Global Geopark, China. *Environ. Earth Sci.* **2018**, *77*, 360. [[CrossRef](#)]
41. Sae-Ju, J.; Chotpanarat, S.; Thitimakorn, T. Hydrochemical, geophysical and multivariate statistical investigation of the seawater intrusion in the coastal aquifer at Phetchaburi Province, Thailand. *J. Asian Earth Sci.* **2020**, *191*, 104165. [[CrossRef](#)]
42. Khan, A.F.; Srinivasamoorthy, K.; Prakash, R.; Rabina, C. Hydrochemical and statistical techniques to decode groundwater geochemical interactions and saline water intrusion along the coastal regions of Tamil Nadu and Puducherry, India. *Environ. Geochem. Health* **2021**, *43*, 1051–1067. [[CrossRef](#)]
43. Schoeller, H. Qualitative evaluation of groundwater resources. *Methods Tech. Groundw. Investig. Dev. UNESCO Water Resour. Ser.* **1965**, *33*, 44–52.
44. Resz, M.A.; Roman, C.; Senila, M.; Török, A.I.; Kovacs, E. A Comprehensive Approach to the Chemistry, Pollution Impact and Risk Assessment of Drinking Water Sources in a Former Industrialized Area of Romania. *Water* **2023**, *15*, 1180. [[CrossRef](#)]
45. Wakida, F.T.; Lerner, D.N. Non-agricultural sources of groundwater nitrate: A review and case study. *Water Res.* **2005**, *39*, 3–16. [[CrossRef](#)]
46. Roy, S.; Gaillardet, J.; Allegre, C.J. Geochemistry of dissolved and suspended loads of the Seine river, France: Anthropogenic impact, carbonate and silicate weathering. *Geochim. Cosmochim. Acta* **1999**, *63*, 1277–1292. [[CrossRef](#)]
47. Fan, B.; Zhao, Z.; Tao, F.; Liu, B.; Tao, Z.; Gao, S.; Zhang, L. Characteristics of carbonate, evaporite and silicate weathering in Huanghe River basin: A comparison among the upstream, midstream and downstream. *J. Asian Earth Sci.* **2014**, *96*, 14–26. [[CrossRef](#)]
48. Liu, J.; Peng, Y.; Li, C.; Gao, Z.; Chen, S. An investigation into the hydrochemistry, quality and risk to human health of groundwater in the central region of Shandong Province, North China. *J. Clean. Prod.* **2021**, *282*, 125416. [[CrossRef](#)]

**Disclaimer/Publisher’s Note:** The statements, opinions and data contained in all publications are solely those of the individual author(s) and contributor(s) and not of MDPI and/or the editor(s). MDPI and/or the editor(s) disclaim responsibility for any injury to people or property resulting from any ideas, methods, instructions or products referred to in the content.